SCIEPublish

Article

Hardness-Porosity-Grain Size Interrelationship in Conventionally Sintered 3 mol% Yttria Stabilized Zirconia

Abhijeet Phatak, Prashant Gupta [†], Somnath Mandal [*,‡], Harshit Agrawal [§], Om Parkash and Devendra Kumar

Department of Ceramic Engineering, Indian Institute of Technology, Banaras Hindu University, Varanasi 221005, India; abhijeet.prajendra.cer11@iitbhu.ac.in (A.P.); Prashant.gupta@wustl.edu (P.G.); harshit.agrawal@iiml.org (H.A.); oprakash.cer@iitbhu.ac.in (O.P.); devendra.cer@iitbhu.ac.in (D.K.)

* Corresponding author. E-mail: smnthmndl@gmail.com or Somnath.Mandal@vesuvius.com (S.M.)

† Present address: Department of Anesthesiology and Washington University Pain Center, Washington University School of Medicine, St. Louis, MO 63110, USA.

‡ Present address: Steel Flow Control Group, Vesuvius Research, Pittsburgh, PA 15205, USA.

§ Present address: Cost and Productivity Reinvention, Accenture Strategy & Consulting, Gurugram 122002, India.

Received: 28 August 2024; Accepted: 8 November 2024; Available online: 14 November 2024

ABSTRACT: Considerable research has been done in the past on expensive, <50 nm particle size 3 mol% yttria-stabilized zirconia (3YSZ) using advanced sintering techniques. However, insights are still needed to reveal which factors among grain size and porosity, when both are changing simultaneously, more strongly control the hardness of conventionally sintered, relatively coarse, 250 nm 3YSZ powder, which can be used to make large industrial engineering ceramic parts at a lower cost. This investigation showed that elevating the sintering temperature from 1500 °C to 1650 °C increased the Rockwell hardness from 49.4 HRA to 86.0 HRA, which was concomitant with an increase in grain size and bulk density. A pseudo-inverse Hall-Petch relationship between hardness and grain size was observed given by H (in HRA) = $153.1 - 69.2/\sqrt{(\text{grain size})}$ with a somewhat low R^2 of 0.95, which was mainly due to the porosity being an additional important variable. Compared to grain size, the impact of open pore fraction (P) on hardness was stronger, inferred from a higher R^2 of 0.99 while fitting the data into the well-known exponential decay equation, $H = 92.9 \exp(-11.1P)$. Finally, it was observed that the 3YSZ conventionally sintered at 1650 °C for 2 h had 0.8% open porosity, 6.08 g/cm^3 bulk density, 960 nm grain size and consisted of only tetragonal ZrO_2.

Keywords: Hardness; Microstructure; Porosity; Sintering; Zirconia

1. Introduction

Yttria-stabilized zirconia (YSZ) is a well-known engineering ceramic material with various strategic applications [1–3]. 3 mol% Y_2O_3 stabilized ZrO_2 (3YSZ), containing ~5.2 wt% Y_2O_3 [4], is used as grinding media and industrial valve guides [2] due to its high hardness, fracture toughness (9 MPa$\sqrt{m}$) and flexural strength. 3YSZ can be processed to nearly zero porosity consisting of only fine grains of tetragonal zirconia phase (no other polymorphs), called tetragonal zirconia polycrystal (TZP) having bending strengths of up to 1200 MPa, with 210 GPa elastic modulus and 10 MPa$\sqrt{m}$ fracture toughness. Due to these exceptional mechanical properties and bio-compatibility, 3YSZ is used as an implant to replace damaged bones [5] and teeth [6]. The low thermal conductivity (2.3 W/mK at 1000 °C), high thermal expansion coefficient (~11×10^{-6} K^{-1}) and stability of the t′-phase makes 4-4.5YSZ (7–8 wt% Y_2O_3) an efficient thermal barrier coating (TBC) for aircraft turbine engines [7]. 8YSZ, composed mostly of the cubic phase, is used in solid oxide fuel cells (SOFC) due to its high ionic conductivity [8]. Balancing ionic conductivity and mechanical stability, 4-5YSZ, containing 65–75% cubic phase, is utilized in automotive gas sensors [9].

Although fully dense YSZ has major engineering ceramic applications, porous YSZ is also valuable and is utilized as ceramic filters, catalyst support, SOFC electrolyte and TBC [10]. For a given YSZ composition, the porosity and proportions of tetragonal and cubic phases can be controlled effectively by altering its thermal processing regime. The

https://doi.org/10.70322/htm.2024.10008

densification of YSZ has been extensively studied in the past. Apart from conventional sintering, advanced techniques such as two-step sintering [11,12], flash sintering [13] and spark plasma sintering (SPS) have been successfully applied [2,14]. Although it is easy to start with a very fine, nanometer-sized powder and fully densify the pressed compact at a lower temperature through conventional sintering, the energy savings may be offset by the high cost of raw materials for certain industries. For instance, using conventional ramp and hold sintering, pressed pellets of 10 nm 1.5YSZ powder were densified to 99% theoretical density upon firing at 1100 °C for 2 h (5 K/min ramp rate) [2], whereas 75 nm 3YSZ attained 98.8% density after sintering at 1500 °C for 1 min [12]. Flash sintering, a rapid process that occurs within seconds, is often limited to small samples and can result in heterogeneous densification and microstructure [15]. The challenge with the SPS process is that it's furnace needs much higher investment than a regular sintering furnace. Fast firing (500 K/min) which has densified 13 nm 3YSZ at 1200 °C in 1 min to 99.2% density with 90 nm grain size [2], may cause thermal shock cracking when subjected to large industrial ceramic parts. Apart from engineering ceramics, zirconia is commonly used in refractories to up to 40 wt% concentration [16–18] as it imparts high-temperature strength and resistance to erosion and corrosion by molten metal and slag. The ramp rate during the firing of such large refractory bricks or nozzles is limited to ~2 K/min [17] to avoid thermal shock. YSZ has low thermal conductivity and a higher thermal expansion coefficient than common refractory oxides like alumina or spinel, so it is even more susceptible to thermal shock. This is because a high thermal shock resistance can be achieved by a high thermal conductivity and a low thermal expansion [17,19].

As many ceramic manufacturing industries need low-cost raw materials [20] and conventional slow sintering, this article used relatively coarse YSZ powder was used, and its densification was studied up to a high temperature correlating it with grain growth and hardness. Hardness is an important parameter, well-correlated with strength, and is important for YSZ's application as grinding media and industrial valves [2,4,21]. This research is also relevant to manufacturing MgO/Y_2O_3 stabilized ZrO_2 refractory tundish nozzles and slide gate plate inserts containing 94–97% ZrO_2 that are fired at temperatures around 1600 °C [22,23]. This study is aimed to reveal whether grain size or porosity has a stronger influence on hardness when both are changing simultaneously. The green binder dosage and the uniaxial pressing procedure were methodically optimized. Phase composition, microstructure and sintering shrinkage were also analyzed.

2. Materials and Methods

3YSZ powder of average particle size 0.25 µm was received from the Defense Research and Development Laboratory, Hyderabad, India. It was analyzed by powder X-ray diffraction (XRD, Miniflex II, Desktop X-ray diffractometer, Rigaku Corporation, Tokyo, Japan) operated over a 2θ range 10–80° with a step size of 0.02°. The raw XRD intensity was converted to the percentage of the maximum intensity (called relative intensity). Then, it was plotted in Origin Pro 2022b software, and a detailed peak list was prepared in Microsoft Excel [24]. Figure 1 shows that tetragonal zirconia (International Center for Diffraction Data Powder Diffraction Files, ICDD PDF 00-050-1089) was the major phase along with some cubic polymorph (ICDD PDF 00-049-1642). The tallest peak of the YSZ powder at 30.28° was closer to tetragonal ZrO_2 (30.27°) than cubic ZrO_2 (30.12°). A peak was considered to be matched when the difference in 2θ of the ICDD PDF from the sample was less than ±0.20° and all these peak position differences for each matched phase were within 0.20° of each other. The peak at 74.28° could not be identified. Monoclinic ZrO_2 (ICDD PDF 00-037-1484) was absent as the 100% intensity peak of it at 28.175° was not found.

Analytical reagent-grade polyvinyl alcohol (PVA) was used as a green binder to press the YSZ powder. To 100 g deionized water at 85 °C, 4 g PVA granules were added and stirred for 3–4 h to obtain a 4% concentration viscous binder solution. In an agate mortar and pestle, the YSZ powder was taken, and 1, 3, 5, 7 and 9 wt% PVA solutions were added. Each separate powder batch was mixed thoroughly and passed 3 times through a 500 µm sieve to obtain moist granules. Following this, they were uniaxially pressed into discs of diameter 15 mm and thickness 0.8 mm at different forming pressures. Green density was then calculated from the weight and dimension and investigated as a function of PVA addition, pressure and dwell time at maximum pressure. After optimizing the pressing conditions, several pellets with a thickness of 4 mm were prepared and subsequently dried at 110 °C for 24 h. Following this, they were sintered in an air atmosphere inside an electrically heated tube furnace (Electroheat, Naskar and Co., Kolkata, India) at temperatures of 1500 °C, 1550 °C, 1600 °C and 1650 °C with a 2 h dwell time. A constant heating and cooling rate of 5 K/min was applied for this process. Linear firing shrinkage was measured from the change in diameter before and after sintering. The bulk density and apparent porosity of sintered pellets were measured by Archimedes technique in boiling water per ASTM C20-00 standard [25]. The phase composition of the samples crushed in an agate mortar and

pestle was studied using XRD. The microstructure of the fracture surface after sputter coating with gold was studied using a scanning electron microscope (SEM, FEI Inspect S50, Amal, Sweden). The average grain sizes were measured using ImageJ software. Finally, Rockwell hardness (SRI RAS PC, Shri Ram Industries, Maharashtra, India) was measured at 588 N load with a diamond indenter.

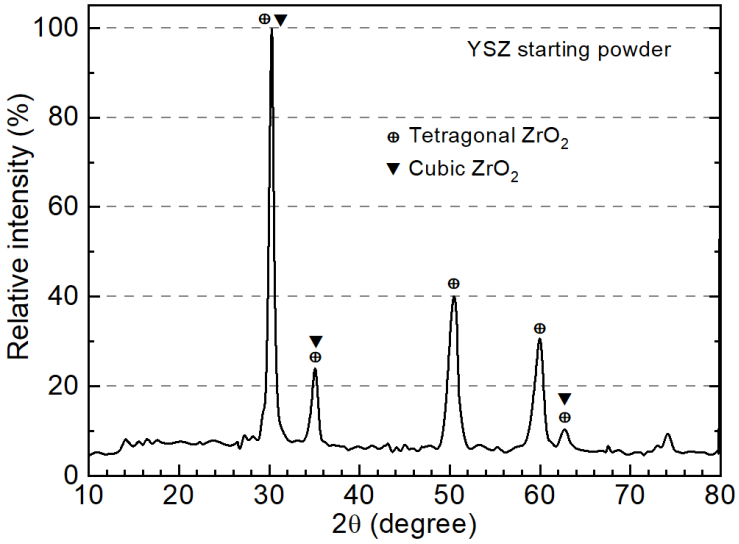

Figure 1. XRD pattern of as received 3YSZ powder.

3. Results and Discussion

3.1. Green Compaction Behavior

Defect-free, dense pressed pellets are crucial to obtain consistent, low-porosity fired ceramics. Figure 2 shows that increasing the PVA content and applying a higher forming pressure increase the green density, consistent with findings from other studies on YSZ [2]. This type of compaction study is often done in the industry whenever a new raw material supplier is used. This is because differences in the starting powder particle size, morphology or processing history can create major variations in the compaction behavior. It was observed that the green densities of pellets with 1%, 3%, 5%, 7%, and 9% PVA, pressed at 261 MPa, were 2.70, 2.76, 2.80, 2.92, and 2.95 g/cm³, respectively. The major phase in the YSZ powder was tetragonal zirconia, which had a theoretical density of 6.13 g/cm^3 (ICDD PDF 00-050-1089). This implied that the green density increased from 44% to 48% upon pressing at 261 MPa when the PVA addition was raised from 1% to 9%. The powder containing 1% PVA was too dry, which is expected as zirconia lacks plasticity (unlike clays), and consequently, the pressed pellet delaminated beyond 261 MPa. This indicated that it had inadequate workability and insufficient green strength. From 5% PVA onwards, an additional trend of flattening of the green density curve with pressure was observed when 305–392 MPa was reached. Excessively high forming pressure provides better compaction but, to the detriment, undergoes more springback. This typically makes green bodies more susceptible to delamination, which becomes prominently visible after firing. Compared to 5% PVA added pellets, the green density with 7% PVA was significantly higher, but 9% PVA did not bring much improvement till 218 MPa forming pressure. Although the addition of green binder gradually enhanced compaction, its burnout during sintering could lead to excessive porosity, potentially reducing mechanical properties such as hardness [17,26,27]. As such, the moderate PVA addition level of 5% was selected, and the dwell time at a maximum pressure of 392 MPa was increased from 20 s to 1 min, which increased the green density from 2.84 g/cm^3 to 2.89 g/cm^3. The final pressing regime for preparing 15 mm diameter and 4 mm thick pellets was loading up to 110 MPa, dwelling for 10 s to de-air, increasing pressure up to 392 MPa and dwelling for 60 s, followed by release.

3.2. Densification

YSZ is known to have high sinterability due to its high oxygen vacancy concentration caused by the substitution of Zr^{4+} ions by Y^{3+} ions, as oxygen is the slowest diffusing species in the crystal structure [21]. This is also observed when a low valency ion substitutes a high valency ion in other oxide ceramics, like MgO-rich $MgAl_2O_4$, where Mg^{2+} substitutes $Al^{3+,}$ producing oxygen vacancies that accelerate sintering [28]. A high % linear firing shrinkage (Figure 3a) of 22.2% was observed in 3YSZ when fired at 1500 °C with a 2 h dwell time. Shrinkage increased steadily to 24.4%

after firing at 1650 °C for 2 h, indicating that densification was active throughout. Bulk density (Figure 3b) increased rapidly from 5.61 g/cm^3 at 1500 °C to 5.98 g/cm^3 at 1600 °C, following which it slowly increased to 6.08 g/cm^3 upon heating at 1650 °C for 2 h, suggesting it had approached final stage sintering. Compared to the theoretical density of tetragonal ZrO_2 (6.13 g/cm^3), this would mean a 99.2% density. Inversely related to bulk density, open porosity reduced from 5.9% after firing at 1500 °C to 0.8% after sintering at 1650 °C for 2 h. Closed porosity, obtained by 100 − (density %) − (open porosity %), was hardly present at that high temperature. These results are reasonably close to the 99.7% density reported for commercial 3YSZ conventionally sintered at 1600 °C for 2 h [29].

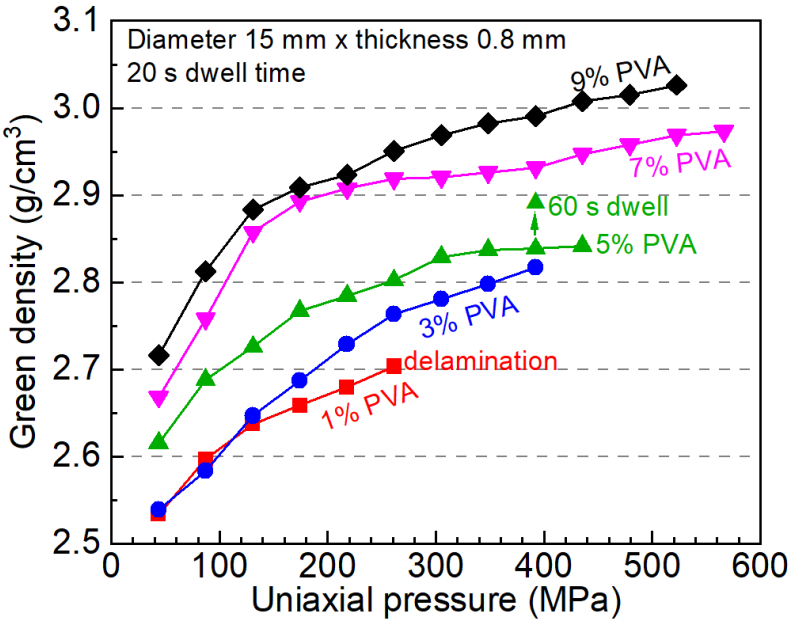

Figure 2. Influence of PVA content and forming pressure on the green density of 250 nm 3YSZ powder at 20 s dwell time. For the optimum PVA content (5%), the effect of increasing dwell time was also studied.

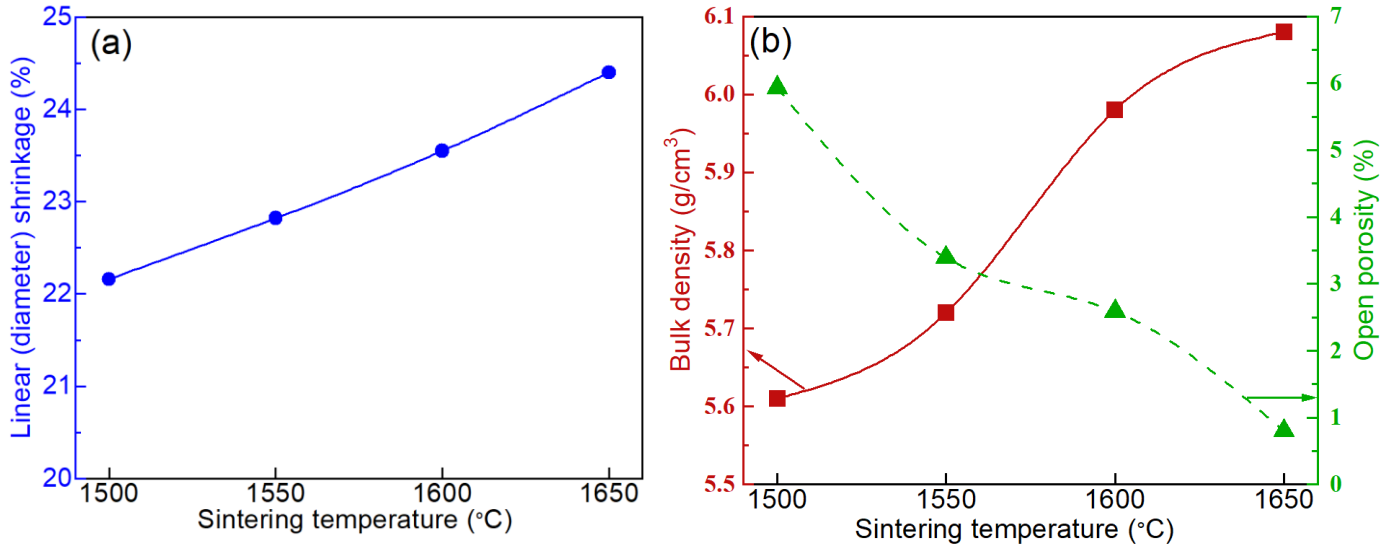

Figure 3. (**a**) Diametral firing shrinkage and (**b**) bulk density and apparent porosity of 3YSZ at different sintering temperatures, each with 2 h dwell time.

3.3. Phase Evolution

The secondary cubic ZrO_2 phase detected in the starting YSZ powder (Figure 1) was seen to disappear upon firing at 1500 °C for 2 h (Figure 4a), forming a desirable, single-phase tetragonal ZrO_2 product. TZP are prized for their high fracture toughness, hardness and strength [2,5,6,21]. The (011) peak of the tetragonal ZrO_2 phase in the sintered material was at a higher angle (30.48° 2θ) than the raw YSZ powder (30.28°) and the ICDD PDF (30.27°), indicating a contraction of the unit cell per Bragg's law [30]. An unidentified peak of 4.3% relative intensity (after subtracting its

immediate baseline noise) remained at 73.28°. It should be noted that grinding in an agate mortar for powder XRD sample preparation can partially reduce the stabilization of zirconia [31,32]. However, all four sintered samples were ground in the same manner. The phase composition of the sintered YSZ remained the same for firing temperatures up to 1650 °C (Figure 4b–d), but the relative intensities of the (112) peak at ~50.5° first increased from 1500 °C to 1550 °C (56.5% to 67.4%) and then gradually reduced after that at 1650 °C (58.8%). Moreover, the (020) peak at ~50.8° was only observed after sintering at 1550 °C and 1650 °C. These two observations suggest that changes in crystal structure may have occurred due to the different sintering temperatures, possibly induced by thermal strain. The monoclinic phase was confirmed to be absent as the 100% intensity peak at 28.175° was not detected in any of the sintered samples. The small unidentified peak at ~73.2° found in the 1500 °C sintered YSZ was also present at 1550 °C and 1600 °C. Apart from these, a small unindexed peak at 28.54° was found after firing at 1550 °C, an unknown peak at 31.6° was observed after heating at 1600 °C, and the 1650 °C sintered sample had two tiny unidentified peaks at 35.02° and 49.62°. Some of these unindexed peaks were close to cubic ZrO_2, but this could not be confirmed due to the absence of the major (111) peak at 30.12°. This may be because the conversion of the tetragonal phase was not fully completed. Finally, a steady shift of the (011) peak of the tetragonal phase was observed when the firing temperature was increased from 1500 °C, 1550 °C, 1600 °C and to 1650 °C (30.48°, 30.48°, 30.42° and 30.38°). This suggested an expansion of the unit cell, which may be caused by the incorporation of more yttria from the cubic phase in the starting material into the tetragonal phase at higher sintering temperatures as the ionic radii of Y^{3+} (0.90 Å) for an octahedral site is larger than Zr^{4+} (0.72 Å) [33].

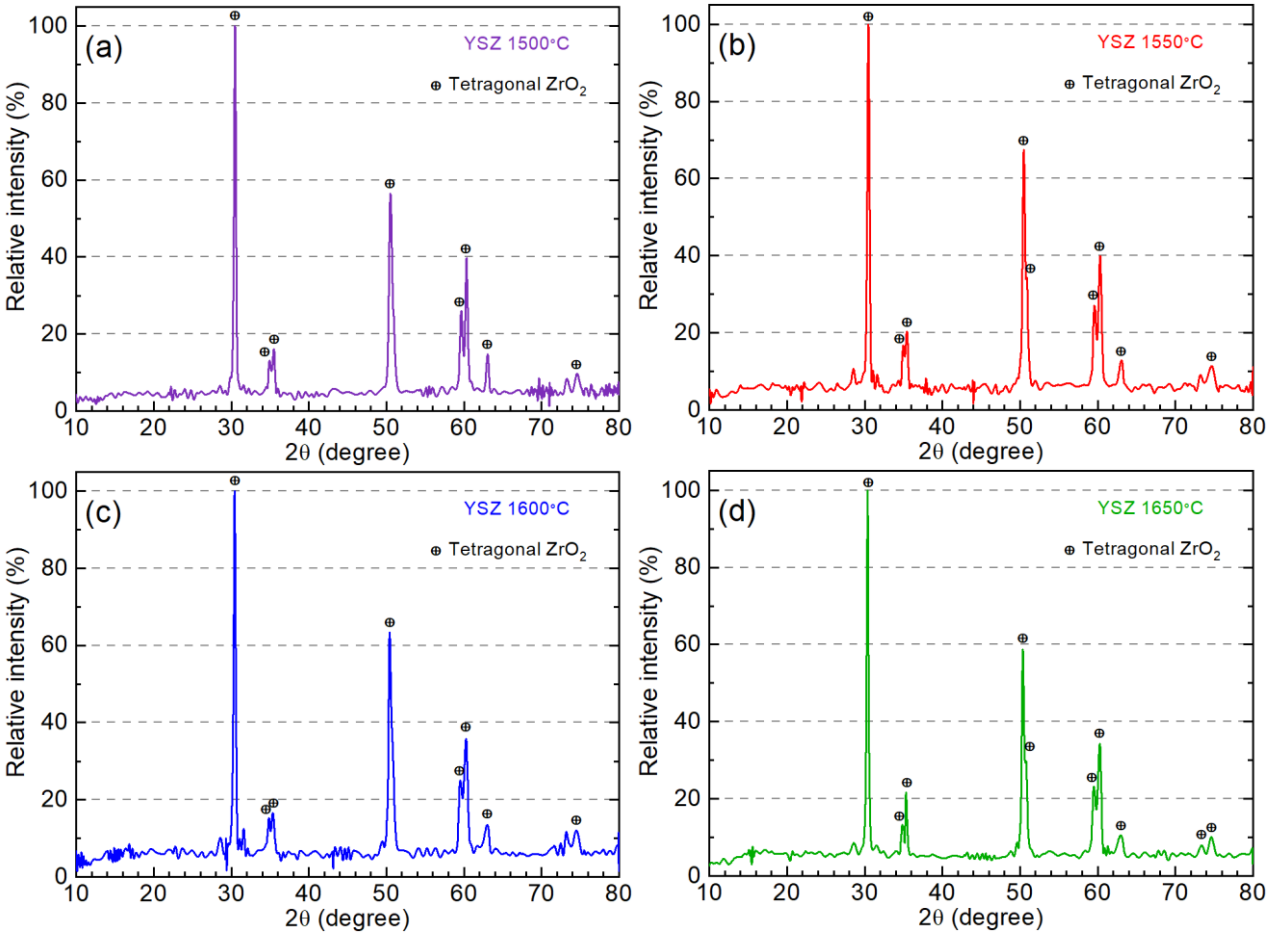

Figure 4. Powder XRD pattern of 3YSZ pellets sintered at (**a**) 1500 °C, (**b**) 1550 °C, (**c**) 1600 °C and (**d**) 1650 °C for 2 h.

3.4. Microstructure

Fracture surfaces are generally preferred over polished surfaces for grain size measurement. The secondary electron image of the fracture surface of YSZ sintered at 1500 °C shows uniformly sized, spherical grains with an average size of 0.44 µm (Figure 5a). This is nearly twice the size of the starting powder (0.25 µm). Some amount of porosity could also be seen. The extensively reported nano-sized [31,34], lenticular- shaped morphology [34] of tetragonal ZrO_2 grains was not observed in this work, possibly due to using a coarser starting powder. Increasing the sintering temperature produced a denser microstructure (Figure 5b–d) with an increase in grain size from 0.57 µm (1550 °C), 0.76 µm

(1600 °C) to 0.96 µm (1650 °C). The grain growth in this article was not very high (not like tens of microns), and a similar grain size was reported by another study [35]. The dense microstructure of Figure 5d correlates well with the low open porosity of 0.8% in Figure 3b.

3.5. Hardness

Figure 6a shows the steady grain growth of YSZ with increasing sintering temperature. Rockwell hardness expressed as scale A values was found to increase rapidly from 49 HRA upon firing at 1500 °C to 62 HRA at 1550 °C, then gradually rose to 69 HRA at 1600 °C and finally improved to 86 HRA at 1650 °C. Similarly, Vickers hardness has been reported to increase with rising sintering temperatures as long as densification continues, after which it tends to drop [36,37]. As higher sintering temperature increased both grain size and hardness simultaneously, it could be mistakenly inferred that hardness was directly proportional to the grain size. This would be in contradiction to the Hall-Petch relation [37,38] given in Equation (1), where H is the hardness, $H_0^{'}$ is the hardness at zero porosity (fully dense material), k is a constant and d is the average grain size.

$$H = H_0^{'} + \frac{k}{\sqrt{d}} \quad (1)$$

The Hall-Petch regime, which means a material becomes harder when the grain size is smaller, has been observed not only in metals but also in oxide ceramics like Al_2O_3, MgO and $MgAl_2O_4$ [39], especially below 1 µm grain size [40]. In fact, it has been observed that 3YSZ follows the Hall-Petch relation for grain sizes > 120 nm [37], but at finer sizes the inverse Hall-Petch relationship is observed, wherein the hardness linearly drops with (grain size)$^{-0.5}$. The breakdown of the Hall-Petch effect at very small grain sizes has been attributed to a change in the deformation mechanism, as reported for 10YSZ when the grain size dropped below 21 nm [40]. The pseudo-inverse Hall-Petch relationship observed in the 3YSZ samples in Figure 6b is unlikely to be real, as the grain sizes are much coarser (437–964 nm) than those reported in the literature. Moreover, the Hall-Petch relationship should be ascertained only for fully dense samples or at least specimens with the same density, although, this is rarely pointed out in publications. It is possible to draw misleading Hall-Petch equation related conclusions from just a plot of hardness and the inverse square root of grain size without delving deeper into the differences in the porosity of the samples. The main intention of this section is to point that out. The deficiency of the pseudo inverse Hall-Petch effect in this study can be seen in the slightly low fitting quality given by a coefficient of determination (COD) or R-squared value of 0.95. The hardness at zero porosity was found to be 153.1 HRA, while the constant, k, was −69.2 HRA$\sqrt{\mu m}$. It must be mentioned that care must be taken while comparing values of the Hall-Petch constants between literature due to the differences in the units of hardness (HRA *vs.* GPa) and grain size (µm *vs.* nm).

The inverse Hall-Petch effect observed in Figure 6b is a false or pseudo-effect, as another crucial variable—porosity—is also changing alongside grain size. The dominant effect of porosity on hardness is presented in Figure 7, where the well-known exponential decay of hardness per Equation (2) is observed. Here H_0 is the hardness of fully dense material, *b* is a pre-exponential constant and *P* is the total pore fraction [27].

$$H = H_0 e^{-bP} \quad (2)$$

The higher quality of fitting of the exponential decay equation (R^2 of 0.99) as compared to the pseudo inverse Hall-Petch regime (R^2 of 0.95) indicates that porosity is stronger as a controlling parameter of hardness than grain size. Figure 7 indicates that the measured hardness varies as H = 92.9 exp(−11.1P). McColm [41] mentioned that compared to regular, phase-stable ceramics that exhibit a constant "*b*" of 7, partially stabilized zirconia, due to its transformation toughening behavior has a higher dependence of Vickers hardness on porosity, expressed by H = 12.27 exp(−8P). The H_0 and *b* constants are not necessarily very different between the current article and McColm's work, as the Rockwell hardness scale A values are quite different than Vickers hardness values. Even with Vickers hardness data, Stevens and Luo [27] had observed different constants (especially the pre-exponential term *b*) than McColm [41] as H = 11.76 exp(−5.03P). Because the fitting quality (R^2) of the pseudo inverse Hall-Petch analysis in this study was lower, and as the former had an inverse square root relation while the hardness and porosity are linked with an exponential decay equation, it can be deduced that porosity has a more dominant effect on hardness of 3YSZ than grain size.

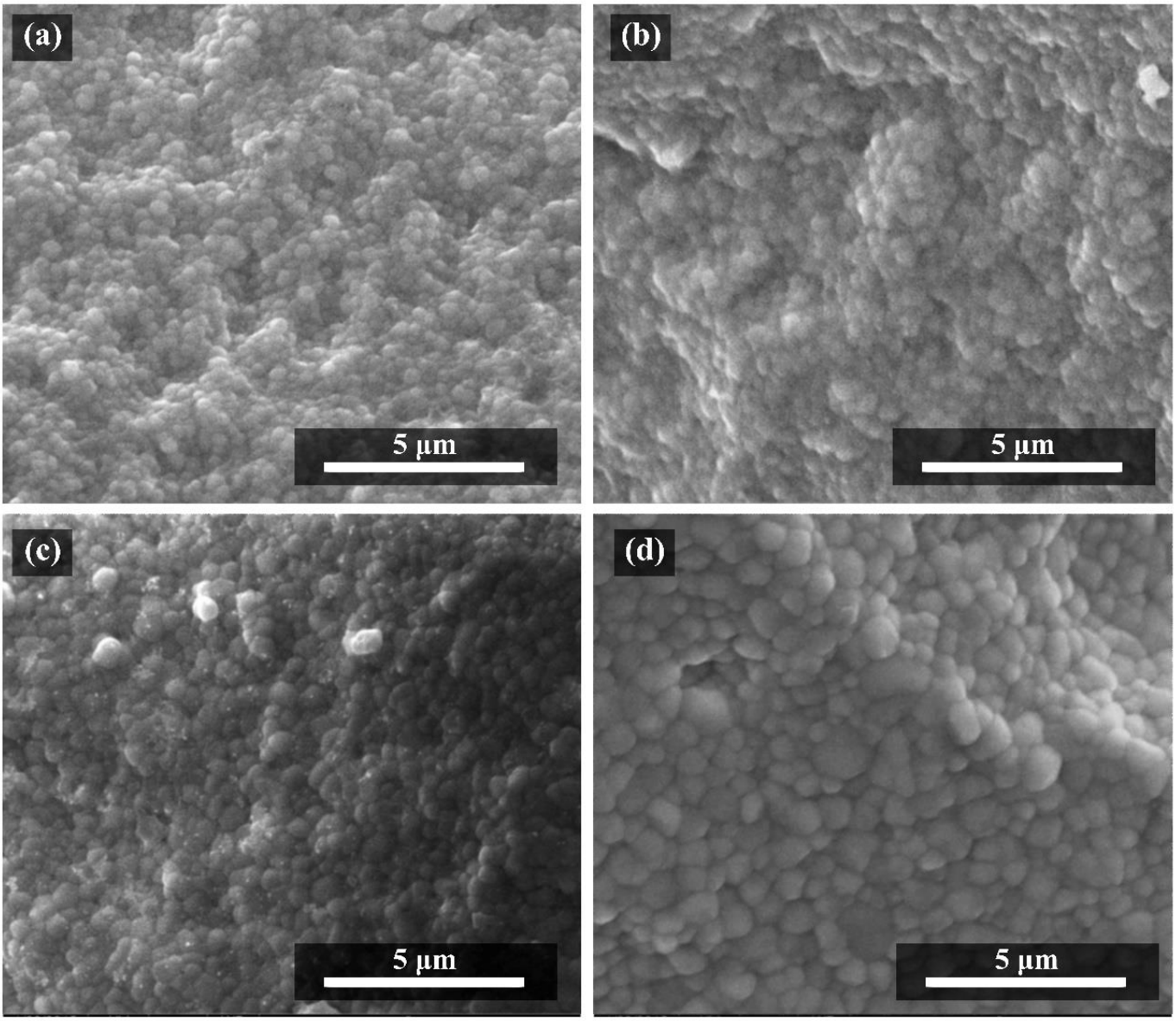

Figure 5. Secondary electron microstructures of the fracture surfaces of 3YSZ after sintering at (**a**) 1500 °C, (**b**) 1550 °C, (**c**) 1600 °C and (**d**) 1650 °C for 2 h.

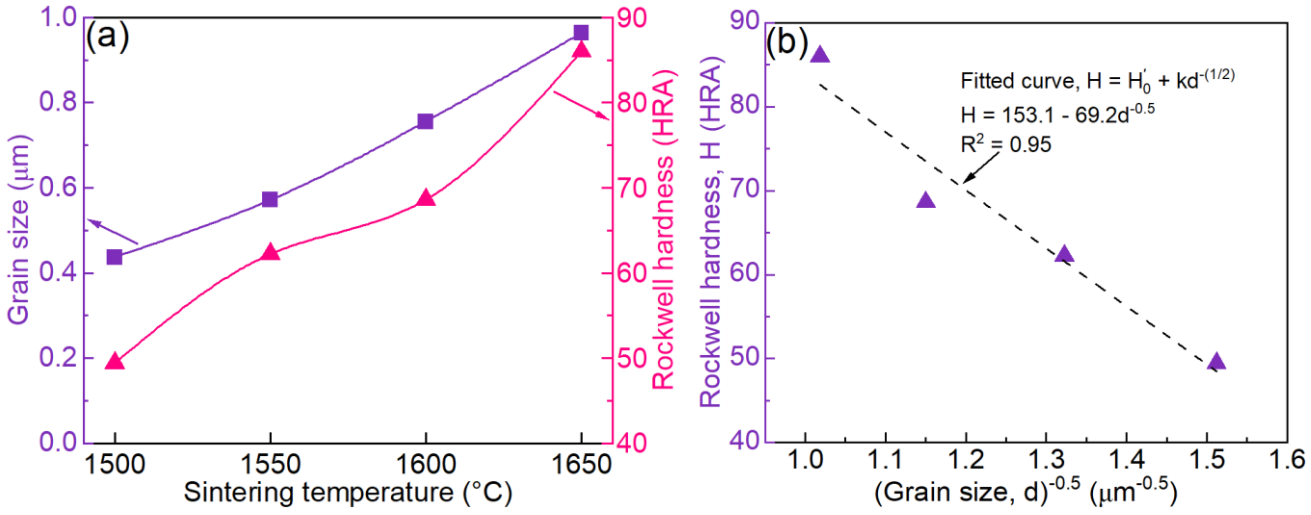

Figure 6. (**a**) Effect of sintering temperature on grain size and hardness of 3YSZ along with (**b**) hardness fitted versus inverse square root of grain size as per inverse Hall-Petch relation.

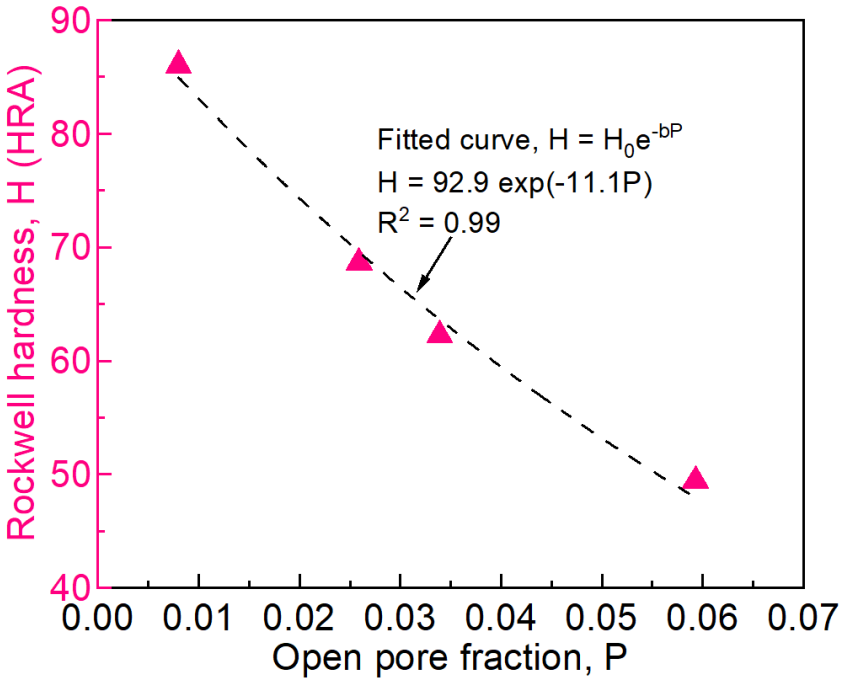

Figure 7. Dependence of hardness on porosity of 3YSZ fitted per the well-known exponential decay equation.

4. Conclusions

Uniaxial pressing of relatively coarse 250 nm 3YSZ powder with 4% concentration PVA solution addition in the range 1–9% revealed that 5% PVA addition with 392 MPa forming pressure with a 1 min dwell time provides an optimum green density of 2.89 g/cm^3. Increasing the sintering temperature from 1500 °C to 1650 °C reduced the open porosity from 5.9% to 0.8%. Firing at 1650 °C for 2 h resulted in a dense 3YSZ with a bulk density of 6.08 g/cm^3, 24.4% firing shrinkage, single phase tetragonal ZrO_2 and a microstructure consisting of spherical grains of average size 0.96 µm. Higher sintering temperatures simultaneously increased Rockwell hardness, grain size and bulk density. A pseudo-inverse Hall-Petch relationship between hardness and grain size was observed, primarily due to the simultaneous variation in porosity. In fact, it was subsequently revealed that porosity had a more dominant effect on hardness than grain size, given by the exponential decay equation, H (in HRA) = 92.9 exp(−11.1P), where P is the open porosity fraction.

Acknowledgments

The authors sincerely thank S. S. Panwar (DRDL, India) for providing 3YSZ powder. S.M. and H.A. are grateful to Ministry of Human Resource Development, India, for providing scholarships during their Masters.

Author Contributions

Conceptualization, S.M. and D.K.; Methodology, S.M.; Software, S.M. and A.P.; Validation, S.M.; Formal Analysis, S.M. and A.P.; Investigation, A.P., P.G., H.A. and S.M.; Resources, D.K. and O.P.; Data Curation, S.M. and A.P.; Writing—Original Draft Preparation, A.P.; Writing—Review & Editing, S.M.; Visualization, S.M. and A.P.; Supervision, D.K. and O.P.; Project Administration, D.K. and O.P.

Ethics Statement

Not applicable as this study did not involve humans or animals.

Informed Consent Statement

Not applicable as this study did not involve humans.

Funding

This research received no external funding.

Declaration of Competing Interest

The authors declare that they have no known competing financial interests or personal relationships that could have appeared to influence the work reported in this paper.

References

1. Phatak A, Gupta P, Mandal S, Agrawal H, Kumar D, Parkash O. Effect of sintering temperature on hardness of dense Yttria-stabilized zirconia ceramics. In Proceedings of the 78th Annual Session of the Indian Ceramic Society, Jamshedpur, India, 2–3 February 2015.
2. Hotza D, García DE, Castro RHR. Obtaining highly dense YSZ nanoceramics by pressureless, unassisted sintering. *Int. Mater. Rev.* **2015**, *60*, 353–375.
3. Hannink RHJ, Kelly PM, Muddle BC. Transformation toughening in zirconia-containing ceramics. *J. Am. Ceram. Soc.* **2000**, *83*, 461–487.
4. MSESupplies. MSE PRO Yttria Stabilized Zirconia Milling Media from MSE Supplies. Available online: https://www.msesupplies.com/products/mse-pro-10-mm-spherical-premium-yttria-stabilized-zirconia-ysz-milling-media?variant=23685767430202 (accessed on 24 August 2024).
5. Piconi C, Maccauro G. Zirconia as a ceramic biomaterial. *Biomaterials* **1999**, *20*, 1–25.
6. Kelly JR, Denry I. Stabilized zirconia as a structural ceramic: An overview. *Dent. Mater.* **2008**, *24*, 289–298.
7. Padture NP, Gell M, Jordan EH. Thermal barrier coatings for gas-turbine engine applications. *Science* **2002**, *296*, 280–284.
8. Minh NQ. Ceramic Fuel Cells. *J. Am. Ceram. Soc.* **1993**, *76*, 563–588.
9. Riegel J, Neumann H, Wiedenmann HM. Exhaust gas sensors for automotive emission control. *Solid State Ionics* **2002**, *152*, 783–800.
10. Zhou J, Wang CA. Porous yttria-stabilized zirconia ceramics fabricated by nonaqueous-based gelcasting process with PMMA microsphere as pore-forming agent. *J. Am. Ceram. Soc.* **2013**, *96*, 266–271.
11. Chen IW, Wang XH. Sintering dense nanocrystalline ceramics without final-stage grain growth. *Nature* **2000**, *404*, 168–171.
12. Mazaheri M, Simchi A, Golestani-Fard F. Densification and grain growth of nanocrystalline 3Y-TZP during two-step sintering. *J. Eur. Ceram. Soc.* **2008**, *28*, 2933–2939.
13. Cologna M, Prette ALG, Raj R. Flash-sintering of cubic yttria-stabilized zirconia at 750°C for possible use in SOFC manufacturing. *J. Am. Ceram. Soc.* **2011**, *94*, 316–319.
14. Khor KA, Yu LG, Chan SH, Chen XJ. Densification of plasma sprayed YSZ electrolytes by spark plasma sintering (SPS). *J. Eur. Ceram. Soc.* **2003**, *23*, 1855–1863.
15. Campos JV, Lavagnini IR, da Silva JGP, Ferreira JA, Sousa RV, Mücke R, et al. Flash sintering scaling-up challenges: Influence of the sample size on the microstructure and onset temperature of the flash event. *Scr. Mater.* **2020**, *186*, 1–5.
16. Mandal S, Mondal S, Das K. Microstructure and phase evolution of Indian magnesite-derived $MgAl_2O_4$ as a function of stoichiometry and ZrO_2 doping. *Int. J. Appl. Ceram. Technol.* **2018**, *15*, 161–170.
17. Mandal S, Dileep Kumar CJ, Kumar D, Syed K, Van Ende MA, Jung IH, et al. Designing environment-friendly chromium-free Spinel-Periclase-Zirconia refractories for Ruhrstahl Heraeus degasser. *J. Am. Ceram. Soc.* **2020**, *103*, 7095–7114.
18. Baudín C, Criado E, Bakali JJ, Pena P. Dynamic corrosion of Al_2O_3-ZrO_2-SiO_2 and Cr_2O_3-containing refractories by molten frits. Part I: Macroscopic analysis. *J. Eur. Ceram. Soc.* **2011**, *31*, 697–703.
19. Schacht CA. *Refractories Handbook*; Marcel Dekker: New York, NY, USA, 2004.
20. Mandal S, Mahapatra MK. Use of dilatometer to screen refractory raw materials. *Int. J. Ceram. Eng. Sci.* **2022**, *4*, 47–52.
21. Butler EP. Transformation-toughened zirconia ceramics. *Mater. Sci. Technol.* **1985**, *1*, 417–432.
22. Zirconia Insert Nozzle, Zirconia Tundish Metering Nozzle from Zirconia Refratech Pvt Ltd. Available online: https://zirconiarefratech.com/InsertNozzle.html (accessed on 12 October 2024).
23. Zirconia Slide Gate Plate Insert from Zirconia Refratech Pvt Ltd. Available online: https://zirconiarefratech.com/SlideGatePlate.html (accessed on 12 October 2024).
24. Jastrzębska I, Piwowarczyk A, Błachowski A, Mandal S. Influence of PbO/CuO ratio on phase composition, microstructure, melt wettability and recyclability of copper slag. *Ceram. Int.* **2024**, *50*, 23315–23330.
25. ASTM International. *C20-00 Standard Test Methods for Apparent Porosity, Water Absorption, Apparent Specific Gravity, and Bulk Density of Burned Refractory Brick and Shapes by Boiling Water*; ASTM: West Conshohocken, PA, USA, 2015.
26. Coble RL, Kingery WD. Effect of Porosity on Physical Properties of Sintered Alumina. *J. Am. Ceram. Soc.* **1956**, *39*, 377–385.
27. Luo J, Stevens R. Porosity-dependence of elastic moduli and hardness of 3Y-TZP ceramics. *Ceram. Int.* **1999**, *25*, 281–286.
28. Ting CJ, Lu HY. Defect reactions and the controlling mechanism in the sintering of magnesium aluminate spinel. *J. Am. Ceram. Soc.* **1999**, *82*, 841–848.
29. Souza RC, dos Santos C, Barboza MJR, Bicalho LDA, Baptista CARP, Elias CN. Fatigue behavior of 3% Y_2O_3-doped ZrO_2 ceramics. *J. Mater. Res. Technol.* **2014**, *3*, 48–54.

30. Tilley RJD. *Understanding Solids*; John Wiley & Sons Ltd: Chichester, UK, 2004.
31. Garvie RC, Hannink RH, Pascoe RT. Ceramic steel? *Nature* **1975**, *258*, 703–704.
32. Reed JS, Lejus AM. Affect of grinding and polishing on near-surface phase transformations in zirconia. *Mater. Res. Bull.* **1977**, *12*, 949–954.
33. Grimes R. Database of Ionic Radii. Available online: http://abulafia.mt.ic.ac.uk/shannon/ptable.php (accessed on 29 November 2022).
34. Sakuma T, Yoshizawa YI, Suto H. The microstructure and mechanical properties of yttria-stabilized zirconia prepared by arc-melting. *J. Mater. Sci.* **1985**, *20*, 2399–2407.
35. Kim SW, Kim SG, Jung JI, Kang SJL, Chen IW. Enhanced grain boundary mobility in yttria-stabilized cubic zirconia under an electric current. *J. Am. Ceram. Soc.* **2011**, *94*, 4231–4238.
36. Xue W, Xie Z, Yi J, Wang C. Spark plasma sintering and characterization of 2Y-TZP ceramics. *Ceram. Int.* **2015**, *41*, 4829–4835.
37. Akhlaghi O, Camposilvan E, Garnier V, Goharibajestani Z, Khabbaz S, Ow-Yang C, et al. Conventional sintering of nano-crystalline Yttria-Stabilized Zirconia enables high-strength, highly translucent and opalescent dental ceramics. *Dent. Mater.* **2024**, *40*, 1031–1040.
38. Callister JW, Rethwisch DG. *Materials Science and Engineering: An Introduction*, 9th ed.; Wiley: Hoboken, NJ, USA, 2014.
39. Wollmershauser JA, Feigelson BN, Gorzkowski EP, Ellis CT, Goswami R, Qadri SB, et al. An extended hardness limit in bulk nanoceramics. *Acta Mater.* **2014**, *69*, 9–16.
40. Feng L, Bokov A, Dillon SJ, Castro RHR. Size-induced room temperature softening of nanocrystalline yttria-stabilized zirconia. *J. Eur. Ceram. Soc.* **2020**, *40*, 2050–2055.
41. McColm IJ. *Ceramic Hardness*; Springer Science+Business Media, LLC: New York, NY, USA, 1990.